Integration between Measurements and Particle Simulations for Hypersonic Rarefied Flows

Takashi Ozawa
Toshiyuki Suzuki
Kazuhisa Fujita

Aerospace Research and Development Directorate
Japan Aerospace Exploration Agency
Chofu, Tokyo 182-8522
JAPAN
ozawa.takashi@jaxa.jp

Abstract

The hypersonic rarefied wind tunnel has lately been developed at JAXA. The characteristics of hypersonic rarefied flows have been investigated experimentally and numerically in this work. Using a sphere pendulous model, the test flow has been probed by measuring its displacement due to the aerodynamic force. In addition, a spatial variation of total pressure of the test flow has also been measured by using total pressure tubes. The flow field from a conical nozzle to a test section was simulated by computational fluid dynamics/direct simulation Monte Carlo loosely coupled computations, and the flow fields were deduced by integrating experimental and numerical results. Consequently, a 25-mm hypersonic rarefied core flow was obtained using a 45-degree conical nozzle with a Mach number greater than 10 and a Knudsen number greater than 0.1.

Key words: HRWT, rarefied gas, aerodynamics, DSMC, hypersonic

Introduction

In order to develop atmospheric reentry systems and planetary entry probes, it is crucial to evaluate the aerodynamic performance of aerospace vehicles in hypersonic flow regime accurately. In the mean time, the Super Low Altitude Test Satellite (SLATS) [1], an engineering test satellite, is under development at Japan Aerospace Exploration Agency (JAXA) so as to improve the resolution for ground observations and reduce the cost for optical systems. The SLATS is operated on the sun-synchronous orbit (SSO) to keep the electric power available for the electric propulsion system, and the target altitude is in a super low earth orbit between 180 and 300 km, where the satellite speed needs to be recovered in order to maintain the satellite altitude. Thus, the assessment of rarefied aerodynamic forces acting on the satellite is important for the SLATS mission. In general, the maximum errors of 10 % and 5 % for force and moment coefficients, respectively, are demanded in these missions.

Thus far, hypersonic aerodynamic prediction has been improved by both ground tests and numerical simulations, especially in continuum flow regime. Aerodynamic forces in free-molecular flow regime can be well-predicted numerically. In transitional hypersonic flow regime, however, we generally rely on direct simulation Monte Carlo (DSMC) [2] computations to estimate rarefied aerodynamic performance for such vehicles since it is difficult and costly to realize rarefied hypersonic test flows equivalent to the flight environments in ground test facilities. State-of-the-art techniques for DSMC simulations are highly sophisticated enough to offer useful information of the rarefied aerodynamics. However, there still remain considerable demands of direct measurement of the vehicle aerodynamics and the heat transfer rate in hypersonic rarefied flows. Besides, the numerical simulations often suffer from inevitable uncertainties originating from accommodation coefficients of

molecules colliding against vehicle surfaces, which are difficult to exactly determine without experiments. Fujita *et al.* [1] investigated details of SLATS aerodynamic characteristics using an analytical method, and found that the aerodynamic coefficients considerably depend on the accommodation parameters of surface materials. Hence, the measurement of accommodation coefficients in hypersonic rarefied flows is necessary to improve the accuracy of aerodynamic prediction on the SLATS.

For these high demands in direct rarefied hypersonic aerodynamic measurements, a pilot model of the hypersonic rarefied wind tunnel (HRWT) [3] has lately been developed at JAXA. This middle-sized wind tunnel is designed to be capable of generating a nominal hypersonic rarefied flow condition; Namely, the flow condition of a Mach number M greater than 10 and a Knudsen number Kn greater than 0.1 is aimed. In order to measure the aerodynamic force in HRWT, it is important to understand characteristics of flow produced by the HRWT accurately. In this work, thus, the rarefied hypersonic flow characteristics of HRWT have been investigated experimentally and numerically. First, a measurement system using a simple pendulous sphere model or total pressure tubes has been developed to probe the hypersonic rarefied gas flows in HRWT. Second, numerical schemes have been developed to simulate the overall HRWT flows. Due to the combined condition of the continuum nozzle flow and the dilute test section, the computational fluid dynamics (CFD) and DSMC methods have been coupled to calculate the HRWT flows. Finally, an integration system between the HRWT measurement and numerical simulations has been developed to improve the understandings of the gas flow characteristics and to measure surface accommodation coefficients on a test model.

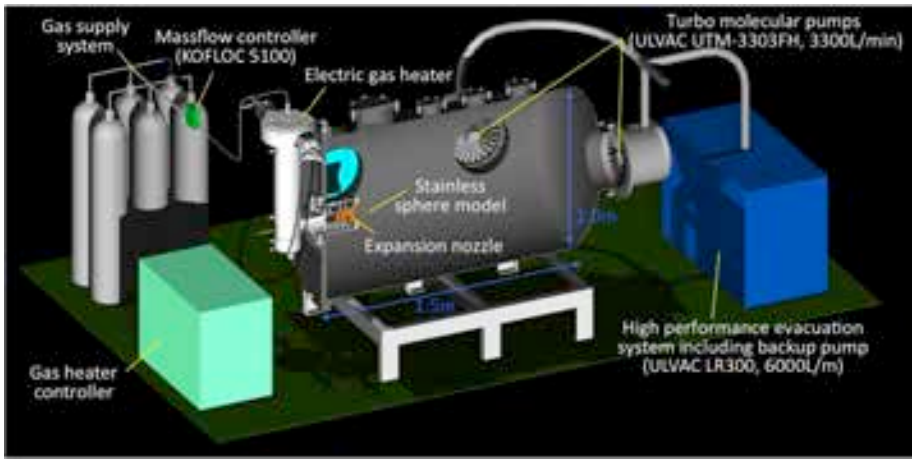

Figure 1 Schematic view of hypersonic rarefied wind tunnel (HRWT).

Experimental Apparatus

A schematic view of the HRWT is shown in Figure 1. The HRWT consists of an expansion nozzle with a large expansion ratio, a vacuum chamber as a test section, and an evacuation system with high exhaust velocity to allow a continuous operation at low ambient pressure. Nitrogen gas from a gas supply system flows into a vacuum chamber through a conical nozzle. The vacuum chamber is 1.0 m in diameter and 1.5 m in length. Three turbo molecular pumps (ULVAC UTM-3303FH, 3.3 m^3/s exhaust capacity) and a back-up dry pump (ULVAC LR300, 0.1 m^3/s exhaust capacity) are equipped in the vacuum chamber. This HRWT pumping system can maintain vacuum pressure in the test section on the order of 1 Pa at a mass flow rate of 0.08 g/s. The static pressure is monitored with a Pirani vacuum gauge (ULVAC GP-1G), a ceramic capacitance monometer (ULVAC CCMH-1A), and a metal ionization gauge (ULVAC GI-M2). These vacuum gauges are mounted on the vacuum chamber.

The HRWT is also equipped with an electric gas heater to increase the flow velocity and the static temperature of flows in the test section. Note that a discharge-less heating system has been selected for HRWT to avoid contamination in the test flow. The electric gas heater consists of a tungsten mesh heater, thermal insulators made of ZrO_2 and Al_2O_3, and a water-cooled outer structure made of stainless steel. The total temperature is monitored at a plenum chamber by using a type-K thermocouple, while a tungsten rhenium alloy wire thermocouple is used to monitor the heater temperature. In order to avoid oxidation of the tungsten mesh heater

at high temperatures, inert gases such as pure nitrogen and noble gases are only allowed to use as the working gas. This heating system is capable of heating the test gas up to approximately 800 K. The nitrogen test gas in the plenum chamber expands into the test section through a conical nozzle. The nozzle throat diameter is 1.632 mm, and the inlet and exit diameters of the nozzle are 25 and 100 mm, respectively. The inlet and outlet half-cone angles are selected to be 45 degree based on our preliminary numerical investigation. The total pressure in the plenum chamber is measured by using a capacitance manometer (ULVAC CCMT-1000D). The temperature of cooling water near the nozzle surface is measured by using a type-K thermocouple, and this temperature is assumed to be identical to the nozzle wall surface temperature in this work.

In order to probe the test flow, a stainless-steel sphere pendulous model with the diameter of 5 mm is inserted into the HRWT flow. Figure 2A shows the typical operation of the test using the sphere model. The sphere model is suspended by a stainless-steel wire to measure the radial distribution of flow properties. The wire has a diameter of 20 μm and a length of 220 mm, respectively. The wire is then connected to a traverse mount which allows triaxial adjustment of the test model position in relation to the test flow. The sphere model is initially set at 17 mm downstream from the nozzle exit and on the nozzle center line. The flexural rigidity of the wire was found negligible compared to aerodynamic forces acting on the model. In addition, total pressure tubes were designed to measure the total pressure distribution in the HRWT test section. A typical operation is shown in Fig. 2B. Two types of tube diameter are tested in this study: One is outer diameter(d_o)/inner diameter(d_i)=2.5/1.5 mm, the other is d_o/d_i=1.6/1.0 mm. Similar to the pendulous model, total pressure tubes are attached to the triaxial stage, and the two-dimensional pressure distributions can be measured. The location of sphere test model and total pressure tube is measured by an image processing technique using a megapixel CCD camera mounted on the quartz window of the test chamber. The original coordinate data is digitized by scanning the photograph, and the experimental uncertainty of the coordinate is estimated to be less than ±0.25 mm.

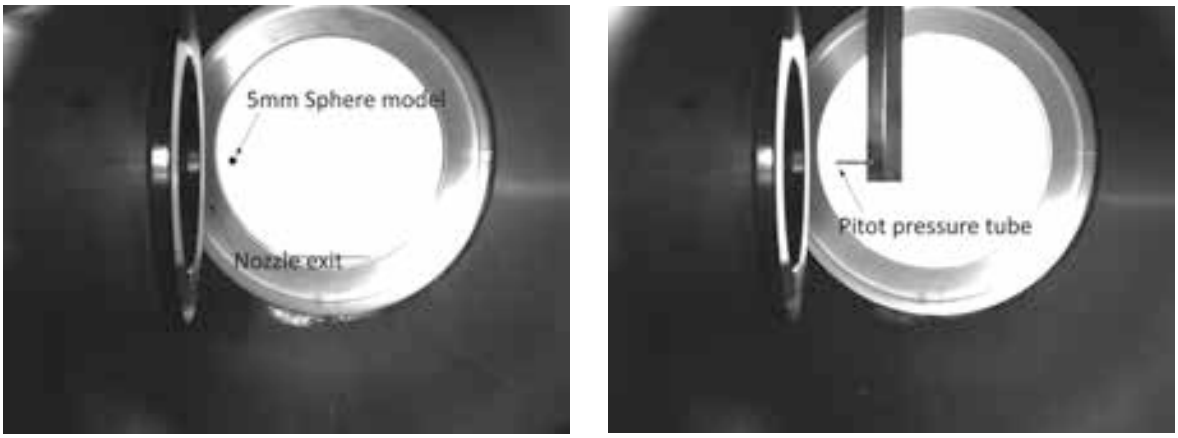

(A) 5mm-sphere pendulous model (B) Total pressure tube

Figure 2 Aerodynamic force measurement system installed in HRWT.

Numerical Flow Modeling

Although the N_2 nozzle flow in the convergence section is so dense that the CFD is capable of calculating the flow field, the flow becomes rarefied in the divergence and test section, where continuum assumption may not be eligible. On the other hand, it is too expensive to simulate the overall section inside the nozzle using the DSMC, and thus, the CFD and DSMC methods are loosely coupled so as to perform the full nozzle flow calculations. The HWRT flow simulations have been performed for the mass flow rate of 0.08 g/s, and the stagnation pressure has been determined accordingly.

CFD calculations in this work were carried out using the JAXA's optimized nonequilibrium aerothermodynamic analysis (JONATHAN) code [4]. In the code, the convective numerical flux is formulated by the AUSM-DV scheme [5] with the second-order upwind-based MUSCL scheme [6]. To settle the strong stiffness originating from chemical reactions, the diagonal implicit scheme [7] is applied to the chemical source terms, whereas the convective and the viscous terms are integrated explicitly in time using local time steps. The collision integrals

in the JONATHAN database are mostly taken from Refs. [8]-[10]. The coefficients of viscosity, thermal conductivity, and ordinary diffusion are computed by the first-order expressions of the Chapman-Enscog theory. The further details of the JONATHAN code can be found in Ref. [11]. In this work, N_2 gas nozzle flows were simulated with respect to each condition inside the nozzle in HRWT. Although a two-temperature model and thermochemical models with several chemical reaction databases were available, neither vibrational excitations nor chemical reactions were considered in this work. To begin with, the nozzle configuration and mesh were generated, and then the convergence-divergence nozzle flow was simulated with a specified total pressure and temperature in the reservoir to fit with the mass flow rate of 0.08 g/s. Only N_2 was considered in the simulations, and for the gas-surface interaction, a non-slip diffuse model was employed.

In this study, the Modeling Of Transitional-Ionized Flows (MOTIF) [12],[13] DSMC code is used to simulate rarefied nozzle flow. In the code, the computational time step is chosen with the one associated with molecular collisions. The no time counter (NTC) scheme [2] is employed for modeling the molecular collision frequency, and the variable hard sphere (VHS) model [2] is used for modeling the collision cross section between particles. The Borgnakke-Larsen (BL) model with temperature-dependent rotational and vibrational relaxation numbers is used for modeling rotation-translation (R-T) and vibration-translation (V-T) energy transfers between neutral species. The Millikan and White (MW) form of the relaxation time are used for V-T rates, and Parker's rates for the R-T rates. For modeling chemical reactions the total collision energy (TCE) model is used, and for modeling electronic excitation transitions, either the quantum-kinetic (Q-K) model or cross section (CS) model is utilized in the code. For the gas-surface interaction modeling, both the Maxwell reflection model and Cercignani-Lampis-Lord (CLL) reflection model are employed. In the Maxwell model, the Maxwell accommodation factor of the surface decides the ratio of a diffuse reflection to a specular reflection. The CLL model assumes no coupling between the normal and tangential components of the velocity during the reflection process. Therefore, three accommodation parameters for normal and tangential velocity and energy fractions are required in this model.

In this work, 3D DSMC calculations were carried out for 100 % N_2 nozzle flows using the MOTIF code. Although the nozzle flow was assumed to be chemically frozen, R-T and V-T energy transfers were considered. Only N_2 species was considered in the flow, and the VHS parameters can be found in Refs. [2] and [14]. The gas-surface interaction was modeled using the Maxwell model, and a diffuse condition with total energy and momentum accommodation with the measured surface temperature was used for the nozzle surface. The time step, cell size, computational domain, and total number of simulated molecules were investigated to obtain results that are independent of these DSMC numerical parameters. Macroparameter sampling is started after a time period that is sufficient to reach the steady state and the total number of time steps used in the sampling is approximately 25,000. The DSMC computational domain extends from approximately 18 mm downstream from the nozzle throat to 150 mm downstream from the nozzle exit. The DSMC inflow boundary condition is given by the converged solution obtained by CFD computation, while the equilibrium condition at the measured ambient pressure is assumed at the outer boundary condition.

In order to consider the effect of flow disturbances due to a test model and calculate the drag on the model from the microscopic viewpoint, it is necessary to integrate the model with DSMC calculations to compute the model displacement more accurately. In DSMC, the force on the model is calculated from the summation of particle momentum transfer during the sampling time as

$$\mathbf{F} = \sum_{p} [(m\mathbf{v}_p^{pre} - m\mathbf{v}_p^{post}) F_{num,p}] / \Delta t \cdot \tag{1}$$

The particle information is accumulated over the sampling time and the force are the average value over the sampling time to reduce the statistical noise. The displacement of the test model is calculated by using the force obtained in Eq. (1) as

$$\theta = \tan^{-1}\left(\frac{F_x}{m_s g - F_z}\right), \tag{2}$$

$$\Delta x = L\sin\theta,\ \Delta z = L(1-\cos\theta), \tag{3}$$

where m_s and L are the mass of the sphere model and the length of the wire sustaining the sphere model, respectively.

In the course of the present DSMC calculation, the sphere model is initially set at 17 mm from the nozzle exit along the centerline in accordance with the HRWT measurement. Once the flow reaches the steady state, the aerodynamic forces acting on the sphere model and the displacement are calculated by using Eqs. (1)-(3). The

sphere model is then moved to a new balanced position, and the DSMC calculation is again carried out. The aerodynamic forces and the displacement are calculated every 3,000 time steps. This iteration is repeated until the amount of displacement becomes less than 10 % of the representative length of the test model (0.25 mm). Note that the test model is placed on the *x*-*z* plane in order to maintain the symmetric condition about the transversal (*y*) direction. The sphere model diameter d_s and the wire length L is set to 5 mm and 220 mm in accordance with the HRWT measurement. In the DSMC code, both the Maxwell reflection model and the CLL reflection model [15] are employed for the test model. The accommodation parameters can be investigated for the dependence on the material, surface temperature, surface roughness, and so forth. In this work, the gas-surface interaction was modeled using the Maxwell model, and two extreme boundary conditions are applied: One is a diffuse condition with total energy and momentum accommodation with a surface temperature of 290 K, and another is a specular condition.

Results and Discussions

From our previous work, it was found that for the accurate estimation of the test model displacement, it is necessary to integrate the test model with the DSMC flow field calculation because the flow disturbance due to the test model is not negligible. Flow-sphere integrated DSMC calculations have been carried out, and the effect of the test model integration has been investigated. Figure 3 shows comparison of Mach number contours between the cases with and without the sphere model. A uniform core flow (M > 10) with a diameter of 25 mm is generated in the test section, and the effect of a sphere model can be seen approximately 10 mm upstream of the sphere. The flow is dramatically decelerated near the model. The core flow speed is approximately 940 m/s without heating, and the displacement is approximately 16 mm. The flow speed decreases around the sphere model, and the sphere model integration in DSMC improved the displacement prediction by 15 % at a maximum.

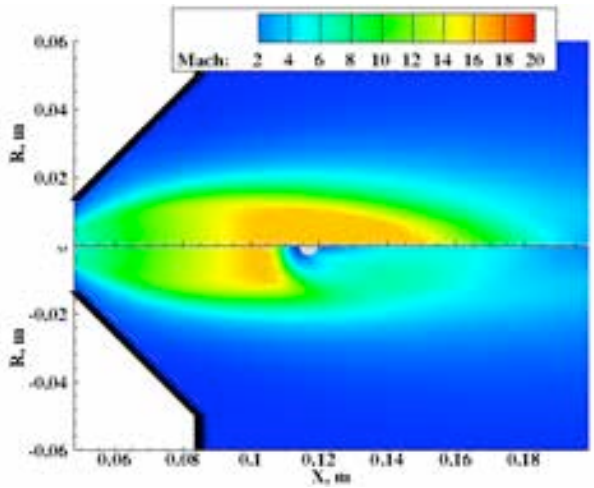

Figure 3 Comparison of Mach number contours between cases with and without a sphere model.

The sphere model displacements due to the aerodynamic forces were investigated along the radial direction. Figure 4 shows comparison of the sphere model displacement between the calculated and measured results for (a) non-heated case (T_0=290 K) and (b) heated case (T_0=750 K) at the mass flow rate of 0.08 g/s. For the calculation, the results are shown for the diffuse and the specular cases. From the measured results, it can be seen that although significant radial change exists in the outer region of the test flow, the displacement of the model is almost constant in the 25 mm core region. From the comparison between Fig. 4A and 4B, one can see that the amount of displacement for the heated case becomes larger than that of the non-heated case. This result is attributed to the increase of flow velocity in the test section with increasing the stagnation temperature. For the heated case, the core velocity is increased by approximately 500 m/s from the non-heated case and becomes faster than 1,200 m/s. From the calculated results shown in Fig. 4A, one can see that the displacement for the diffuse condition becomes larger than that for the specular condition for all radial position. Almost the same situation can be seen in Fig. 4B. This trend can be explained as follows: In the present study, the surface temperature of sphere model is assumed to be 290 K. For the diffuse condition, N_2 molecule striking on the sphere model surface completely accommodates with the model surface temperature of 290 K. For this case, the average speed of reflected molecule for diffuse condition is mostly smaller than that for specular condition. As a

result, the number density of N_2 molecule for the diffuse case becomes higher than that for specular one, resulting in higher dynamic pressure acting on the model for the diffuse case. For these reasons, the model displacement becomes higher with the diffuse wall compared to that with the specular wall.

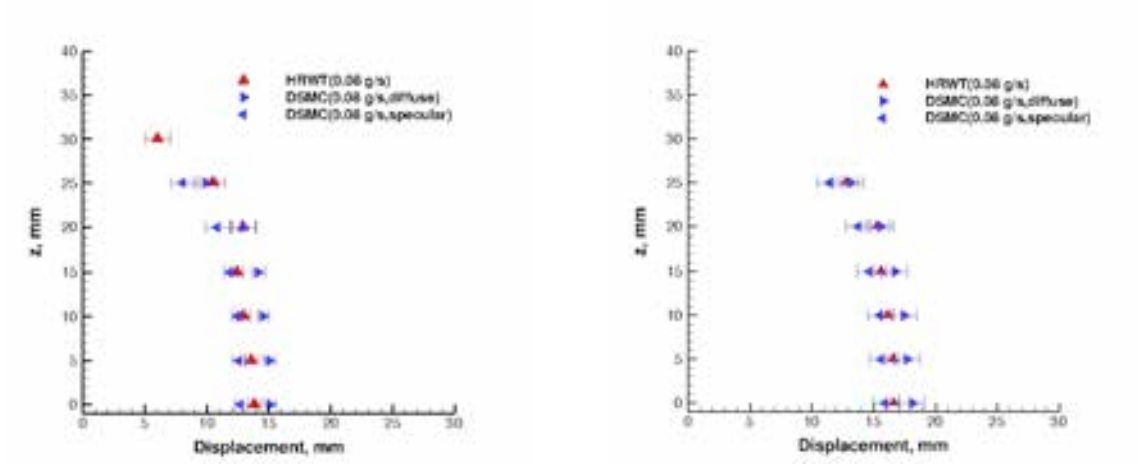

(A) non-heated case (B) heated case

Figure 4 Comparison of sphere model displacement between calculation and measurement at 17 mm downstream from the nozzle exit.

From the comparison between the calculation and the measurement in Fig. 4, good agreement can be seen between the measured and computed results because the measured displacement is located between the DSMC specular and diffuse calculations. Base on this result, it is believed that the present numerical method can reproduce the characteristics of the HRWT flows within the uncertainty originating from the accommodation factor of molecules colliding against the sphere model. Note that slight discrepancy can be seen in the outer region of the core flow in Fig. 4A. The increase in the measured displacement near z = 20 mm is caused by the interaction among the core flow development, boundary layer development, and the background pressure, which is approximately 1.4 Pa. In the DSMC computations, this phenomenon is slightly under-estimated. One possible reason for this may come from the difference in the boundary layer thickness between the calculation and the measurement. In general, the nozzle wall surface might be rough compared with an ideal wall surface assumed in the DSMC calculation. In order to examine the hypothesis about the boundary layer thickness, the DSMC calculation was further performed by changing the boundary layer thickness artificially [16]. From this investigation, it was confirmed that the thickness of boundary layer becomes larger and the core flow diameter becomes smaller with increasing the surface temperature of the nozzle. It was also found that the dynamic pressure around the flow center becomes higher when the boundary layer becomes thicker. Correspondingly, the flow field around the sphere model was re-calculated by correcting the boundary layer thickness, and the sphere model displacement was re-estimated. The agreement between the calculation and the measurement was improved, and the measured displacement became between the DSMC specular and diffuse results. Note that no evidential result for condensation to liquid state was obtained in the cases under consideration, even though the flow temperature is believed to be below dew point temperature especially for the non-heated case. This trend is believed to occur because the Knudsen number remains at the order of 0.1 due to the low density of test flow. In order to avoid this peculiar discussion, the gas heater system will be improved so that the test flow temperature in the test chamber could be higher than the dew point temperature in the future.

The total pressure distributions in the test section were investigated by using the total pressure tubes. Using the total pressure tube of 2.5 mm outer diameter, total pressure distributions were measured with an interval of 5 mm for cases (A) and (B). In Fig. Figure 5, the measured total pressure distributions are compared with the computed dynamic pressure. The obtained results are shown in Fig. 5A for the non-heated case (A) and in Fig. 5B for the heated case (B). For case (A), a trend of pressure increase in the interaction region between the core flow and the background gas can be seen clearly in both the measured and computed results. This trend is decreased for the 750 K case. From the measured results shown in Fig. 5, it can be seen that the total pressure near the nozzle exit for case (B) becomes higher than that for case (A). This feature is due to the increase of the flow velocity with increasing the stagnation temperature. In Fig. 5, calculated dynamic pressure distributions around the nozzle exit are also shown for the purpose of comparison. In order to compare the calculated results with experimental data directly, total pressure needs to be calculated from the numerical results so that the

calculated total pressure can be viewed as the pressure that would be obtained if a total pressure tube were put into the computed flow field. Following the study in Refs. [17] and [18], the total pressure is calculated by taking account of the effect of rarefaction as follows:
(1)Total pressure behind a shock wave is first calculated by using the calculated static pressure with the Rayleigh pitot tube equation [19] as

$$p_{02}/p_1 = \left[\frac{(\gamma+1)^2 M^2}{2(2\gamma M^2-\gamma+1)}\right]^{\frac{\gamma}{\gamma-1}} \frac{2\gamma M^2-\gamma+1}{\gamma+1}. \quad (4)$$

(2)The measured total pressure, p_{0m}, is finally obtained by taking account of the effect of rarefaction as

$$\log_{10}(p_{0m}/p_{02}) = a - b\log_{10}(\mathrm{Re}_2), \quad (5)$$

where the probe Reynolds number behind a shock wave is calculated using the actual diameter of the pressure tube (d_p) as

$$\mathrm{Re}_2 = \rho_2 u_2 d_p/\mu_2. \quad (6)$$

Because the experimental condition and the tube diameter in this study are different from those in the work of Boyd *et al.* [17], the degree of rarefaction of the present study seems to be different from those conditions. For this reason, the constant parameters in Eq. (5) are determined independently in this study. The parameters used in this study are summarized in Table 1.

Table 1 Parameters used in Eq. (5)

Parameters	290 K	750 K
a	0.3	0.05
b	0.5	0.5

The computed total pressure are compared with the measured one in Fig. 6A for case (A), and in Fig. 6B for case (B). In Fig. 6, two pressure tube results for the d_o of 2.5 mm and 1.6 mm, respectively, are presented. It can be seen in the figure that the differences in tube outer diameter between 2.5 and 1.6 mm are clearly seen in both computed and measured results. The overall agreement between computed and measured results are considerably good except for a slight difference for case (A) with the 1.6-mm outer diameter tube. The difference may be attributed to the slight increase in the stagnation pressure during the measurement.

From the experimental and numerical results about the sphere model and the total pressure tube, it is considered that the present numerical method can reproduce the major characteristics of the test flows in HWRT. The flow Mach number and the Knudsen number for mass flow rate of 0.08 g/s are estimated by numerical results, and the obtained results are presented in Fig. 7. As shown in Fig. 7, the core flow diameter is estimated to be roughly 25 mm. For case (A), although the flow Mach number is higher than 10, the Knudsen number remains below 0.1. On the other hand, the flow Mach number of 16 and the Knudsen number of 0.2 are achieved for case (B).

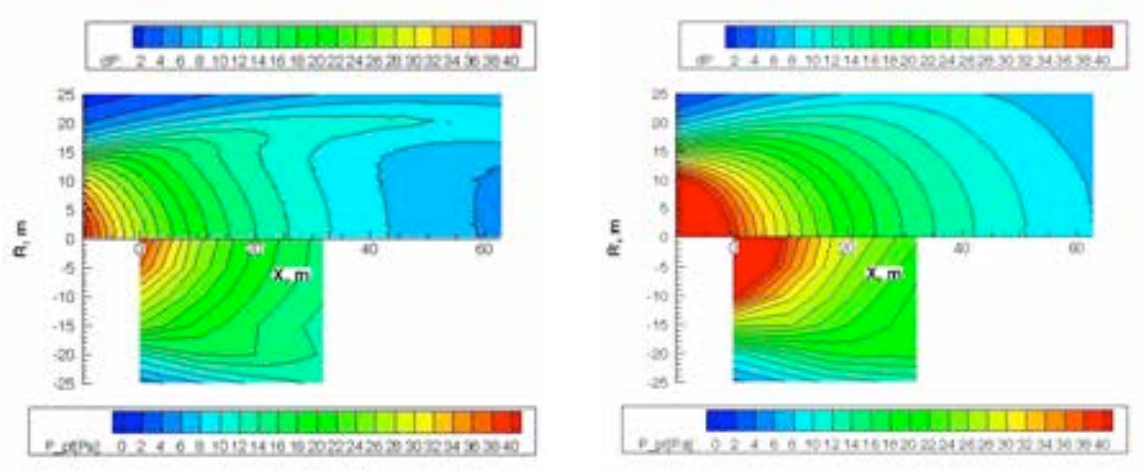

(A) non-heated case (B) heated case

Figure 5 Comparison of computed dynamic pressure (top) and measured total pressure (bottom).

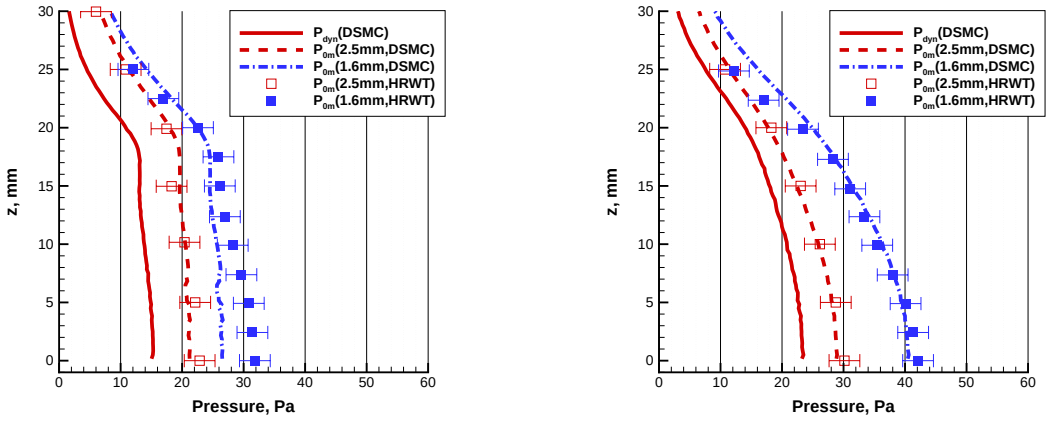

(A) non-heated case (B) heated case

Figure 6 Comparison of computed and measured total pressure profiles along radial direction at 17 mm downstream from the nozzle exit.

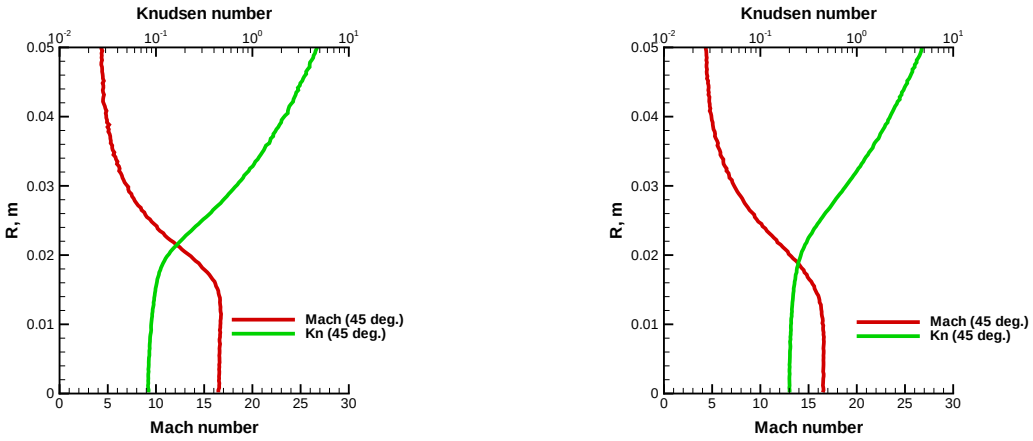

(A) non-heated case (B) heated case

Figure 7 Mach number and Knudsen number distributions along the radial direction at 17 mm downstream from the nozzle exit.

Conclusions

Flow characteristics of HRWT have been investigated by using the pendulous sphere model and the total pressure tubes. Using the CFD/DSMC numerical approach integrating with the HRWT test model, we analyzed the major characteristics of the test flows in HRWT. It was found that the test flows are well-represented by the numerical approach, and the heating effect increases the Knudsen number in the test section. With the heater activated, the free stream Mach number greater than 10 and Knudsen number of 0.1 are achieved in the 25mm-core flow region.

References

[1] K. Fujita and A. Noda, Rarefied Aerodynamics of a Super Low Altitude Test Satellite, AIAA Paper 2009-3606, 2009.

[2] G. A. Bird, Molecular Gas Dynamics and the Direct Simulation of Gas Flows, Clarendon, Oxford, England, U.K., 1994.

[3] K. Fujita, T. Suzuki, T. Ozawa, Development of a Pilot Model of Hypersonic Rarefied Wind-Tunnel, in 27th International Symposium on Rarefied Gas Dynamics, AIP Conference Proceedings, Vol. 1333, pp. 407-412, 2010.

[4] K. Fujita, S. Matsuyama, and T. Suzuki, Prediction of Forebody and Aftbody Heat Transfer Rate for Mars Aerocapture Demonstrator, AIAA Paper 2012-3001, 2012.

[5] Y. Wada and M. S. Liou, A Flux Splitting Scheme with High-Resolution and Robustness for Discontinuities, AIAA paper 1994-0083, 1994.

[6] B. van Lee, Toward the Ultimate Conservative Difference Scheme. 5, A Second-Order Sequel to Godonov's Method, Journal of Computational Physics, Vol. 23, No. 1, pp. 101–136, 1979.

[7] S. Eberhardt and S. Imlay, Diagonal Implicit Scheme for Computing Flows with Finite Rate Chemistry, ournal of Thermophysics and Heat Transfer, Vol. 6, No. 2, pp. 208–216, 1992.

[8] C. Park, R. L. Jaffe and H. Partridge, Chemical-Kinetic Parameters of Hyperbolic Earth Entry," Journal of Thermophysics and Heat Transfer, Vol. 15, No. 1, pp. 76–90, 2001.

[9] M. Capitelli, C. Gorse, S. Longo and D. Giordano, Collision Integrals of High-Temperature Air Species, Journal of Thermophysics and Heat Transfer, Vol. 14, No. 2, pp. 259–268, 2000.

[10] E. Levin and M. J. Wright, Collision Integrals for Ion-Neutral Interactions of Nitrogen and Oxygen, Journal of Thermophysics and Heat Transfer, Vol. 18, No. 1, pp. 143–147, 2004.

[11] K. Fujita, T. Sumi, T. Yamada and N. Ishii, Heating Environments of a Venus Entry Capsule in a Trail Baloon Mission, Journal of Thermophysics and Heat Transfer, Vol. 20, No. 3, pp. 507–516, 2006.

[12] T. Ozawa, T. Suzuki, H. Takayanagi and K. Fujita, Investigation of Martian-Dust Drag and Heat Transfer for Mars Sample Return Mission, Journal of Thermophysics and Heat Transfer, Vol. 25, No. 3, pp. 341–353, 2011.

[13] T. Ozawa, T. Suzuki, H. Takayanagi and K. Fujita, Analysis of Non-Continuum Hypersonic Flows for the Hayabusa Reentry, AIAA Paper 2011-3311, 2011.

[14] G. C. Maitland, Critical Reassessment of Viscosities of 11 Common Gases, Journal of Chemical and Engineering Data, Vol. 17, No. 2, pp. 150–156, 1972.

[15] M. O. Hedahl and R. G. Wilmoth, Comparison of the Maxwell and CLL Gas/Surface Interaction Models Using DSMC, NASA TM-110205, 1995.

[16] T. Suzuki, T. Ozawa and K. Fujita, Experimental and Numerical Study of Flow Diagnostics in Hypersonic Rarefied Wind Tunnel in JAXA, AIAA Paper 2012-0370, 2012.

[17] I. D. Boyd, P. F. Penko, D. L. Meissner and K. J. DeWitt, Experimental and Numerical Investigations of Low-Density Nozzle and Plume Flows of Nitrogen, AIAA Journal, Vol. 30, No. 10, pp. 2453–2461, 1992.

[18] W. B. Stephenson, Use of the Pitot Tube in Very Low Density Flows, AEDC-TR-81-11, Arnold, AFS, TN, 1981.

[19] A. H. Shapiro, The Dynamics and Thermodynamics of Compressible Fluid Flow, Ronald Press, New York, 1953.